Materials Research Express 4(6) (2017) 065501

Zr-doped TiO_2 as a thermo-stabilizer in plasmon-enhanced dye-sensitized solar cells

Anastasia Pasche,[a] Bernd Grohe,[a] Silvia Mittler,[a,b] Paul A. Charpentier[a,*]
[a]The University of Western Ontario, Faculty of Engineering, Department of Chemical and Biochemical Engineering, London, Ontario, Canada, N6A 5B9
[b]The University of Western Ontario, Faculty of Science, Department of Physics and Astronomy, London, Ontario, Canada, N6A 3K7

Abstract. Harvesting solar energy is a promising solution towards meeting the world's ever-growing energy demand. Dye-sensitized solar cells (DSSCs) are hybrid organic-inorganic solar cells with an enormous potential for commercial application, but are plagued by inefficiency due to their poor sunlight absorption. Plasmonic silver nanoparticles (AgNPs) have been shown to enhance the absorptive properties of DSSCs, but their plasmonic resonance can cause thermal damage resulting in cell deterioration. Hence, the influence of Zr-doped TiO_2 on the efficiency of plasmon-enhanced DSSCs was studied, showing that 5 mol % Zr-doping of the photoactive TiO_2 material can improve the photovoltaic performance of DSSCs by 44 %. By choosing three different DSSC designs, it became clear that the efficiency enhancing effect of Zr strongly depends on the closeness of the Zr-doped material to the plasmonic AgNPs.

Keywords: solar cells, DSSCs, Ag nanoparticles, plasmonics, thermo-stabilization, titania, TiO_2, Zr-doping

***Paul A. Charpentiert, E-mail: pcharpen@uwo.ca

1 Introduction

Dye-sensitized solar cells (DSSCs) are regarded as one of the most promising solar cell designs amongst third-generation photovoltaic (PV) technologies, particularly due to their low cost, easy preparation, and minor environmental impact with respect to earlier-generation devices[1,2]. The photoactive semiconductor material is typically TiO_2 in nanoparticle form ($nTiO_2$). Advances in their design,[3-5] their incorporation onto flexible substrates[6-9] and their scalable fabrication techniques[10,11] have allowed DSSCs to move from the laboratory scale to real-life application. Although their positive inherent features can facilitate their entry into the PV market, there is still a need for improvement to achieve higher performance DSSCs. In other words, an increase in DSSC efficiency is desired. One of the biggest challenges for efficiency enhancement is the

inefficient sunlight absorption in DSSCs.[12] The dye that sensitizes the TiO_2 photo-absorbing material does not respond equally to all incoming wavelengths of the solar spectrum,[13] thus limiting the number of photons that can be converted into electricity.

One approach to improve DSSCs light harvesting capabilities is the implementation of plasmonics, typically in form of coinage metal nanoparticles (NPs).[14] These plasmonic NPs offer a resonance phenomenon involving the oscillation of the free electron gas in the metal NP, which is driven by the incoming electro-magnetic wave. This leads to very strong absorption and scattering, and to a highly amplified evanescently decaying electro-magnetic field at the NP's surface[15-17]. The effect is called localized surface plasmon resonances (LSPR). In DSSCs, the NPs increase the effective absorption cross-section by scattering off the incoming photons of their path, thus enhancing the interaction length with the device and by efficiently coupling the amplified evanescent fields to the semiconductor and the dye.[12]

For solar energy harvesting, visible light (400 - 700 nm) is of interest. AgNPs exhibit a strong LSPR effect in the visible range of the solar spectrum.[18-20] These unique optical properties of AgNPs enhance the light absorption capability of their surrounding environment; and several examples have been published that demonstrate enhanced photocurrents in PV devices owing to AgNP's unique absorptive and scattering capabilities.[18-21]

On the other hand, absorption, and especially LSPR, is a well-known mechanism for energy dissipation in form of heat, which is used, e.g., in biodiagnostics, therapy, and drug delivery.[22] Baffou and Quidant[23] have calculated the temperature profile of metal NPs under continuous-wave illumination. They found that the heat density can be greatly non-uniform within a NP. However, at equilibrium, the temperature is generally uniform inside the NP. This behaviour is caused by the much larger thermal conductivity of the metal NP in comparison to the (typically non-metal)

surrounding material. The NP's temperature enhancement depends on several parameters (absorption cross-section, shape of the NP, thermal conductivity of the surrounding medium, wavelength and irradiance of the incoming light, and the distance to the nearest neighboring NPs). For an isolated, spherical (20 nm in diameter: Ø) AuNP in H_2O, which is illuminated at a wavelength of 530 nm at an irradiance of $1 mW/\mu m^2$ a temperature increase of 5°C can be measured. However, when NPs get close to each other e.g., AuNPs (Ø: (30 ± 3) nm) with distances of (100 ± 10) nm to neighboring NPs, the temperature enhancement can be 100°C ($1 mW/\mu m^2$, λ = 532 nm).[23,24]

There is quite a variety of organic dyes that are implemented in DSSCs.[25,26] But ruthenium complex compounds, in particular, have received high interest as photosensitizers in DSSCs, as they show favorable photo-electrochemical properties and a high stability in the oxidized state.[27,28] However, despite these properties heat damage of ruthenium sensitizers has been reported.[29] Increasing dye degradation temperatures (80 - 160°C) in DSSCs lead to unfavourable growth of electron recombination rates, decreasing photo-current densities, and drastically reduced open-circuit voltages (V_{OC}): all contributing to substantially reduced energy conversion efficiencies (η).[30]

AgNPs exhibit very similar temperature enhancements compared to AuNPs,[31] and are therefore excellent candidates to exploit the thermostabilizing effect of zirconium-doped TiO_2 as photoactive material in plasmon enhanced DSSCs. Zirconium (Zr) is one of the most suitable dopants, as it is known to have very high thermo-stabilizing properties. The implementation of Zr-doped TiO_2 NPs ($Zr/nTiO_2$) in the photoactive layer of DSSCs has shown a significant influence on the thermal stability of the semiconducting oxide's specific surface area (SSA) and pore structure, a stabilization of the anatase phase and avoiding the anatase-rutile phase transition at

elevated temperatures, and has consequently enhanced the DSSC performance.[32-38] These factors might be of great benefit in facilitating the heat created by LSPR.

Although AgNPs have been shown to amplify absorption in DSSCs, there is a clear limitation of this enhancement, due to the creation of heat. For example, Qi et al.[21] have observed a decrease in energy conversion efficiency of their fabricated DSSCs when the concentration of AgNPs exceeded 0.6 wt.%. This effect defines an upper limit of the amount of AgNPs that can be incorporated into DSSCs, thus imposing a limit on the cell's absorption improvement. Other researchers have been reporting doping limits as well when incorporating plasmonic nanostructures into their photoactive systems, or simply did not attempt concentrations above 0.5 wt.%.[17,39,40] There are very few studies addressing a moderation by plasmonic-NP doping limits.

The use of Zr as a thermo-stabilizer in plasmon-enhanced DSSCs has yet to be investigated, despite the evidence that this material increases thermal stability by preserving the TiO_2 structure at high temperatures.[41,42] This work examines the effects of incorporating Zr into the $nTiO_2$ photoactive material in LSPR-enhanced DSSCs, with the goal to stabilize the $nTiO_2$ at elevated temperatures (occurring because of plamonic heating effects), to increase the limit of AgNP concentration in the photoactive layer without provoking negative effects on the cell efficiency, and to increase the overall efficiency in energy conversion.

2 DSSC Architecture Design

To understand both the role of Zr and the role of the positioning and distribution of AgNPs in DSSC efficiencies, three different cell-architectures were designed (Fig.1): a) $nTiO_2$ or $Zr/nTiO_2$ as the photoactive material between a standard transparent fluorinated tin oxide (FTO) working electrode (photo-anode) and a Pt counter-electrode as the *classic* architecture without plasmonic

features, b) $nTiO_2$ or $Zr/nTiO_2$ as the matrix containing *random*ly mixed nano-aggregates of AgNPs in Zr-free TiO_2 ($Ag/nTiO_2$), sandwiched between the two electrodes, and c) $nTiO_2$ or $Zr/nTiO_2$ as the matrix between two electrodes, one of which is the photo-anode carrying a layer of AgNPs covered by a *blanket* of Zr-free TiO_2. The *italic* expressions are used throughout the paper to name the designs. The *random* and *blanket* designs (Fig.1) offer different strategies (location and density of the AgNPs) to couple the plasmonics of the AgNPs to the $nTiO_2$ or $Zr/nTiO_2$ photoactive semiconductor material and to investigate the influence on thermo-stabilization. The *random* approach consists of AgNPs (randomly present in a Zr-free nano-agglomerate of $nTiO_2$, in Fig.1 indicated as randomly positioned AgNPs in the photoactive layer) positioned randomly and relatively sparse throughout the entire photoactive material of the DSSC, whereas the *blanket* design consists of pure AgNPs immobilized chemically with a relative high density only on top of the photo-anode via poly(4-vinylpyridine (P4VP). The interaction of the incoming light and the $Zr/nTiO_2$ with the AgNP is different in both designs. The heat production due to LSPR should also be different.

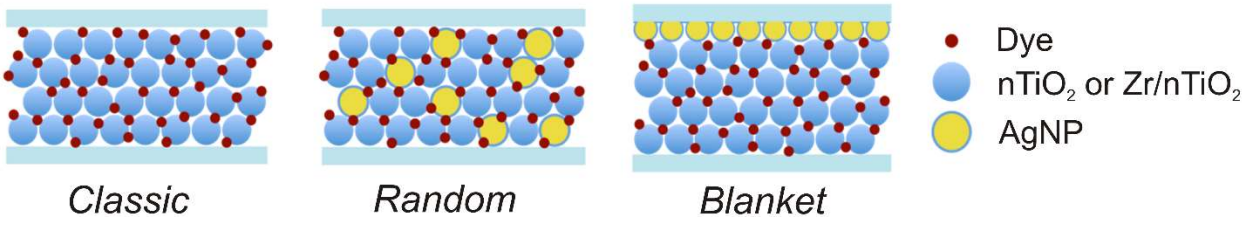

Fig. 1 Schemes of the three DSSC designs. Left: non-plasmonic AgNP-free $nTiO_2$ or $Zr/nTiO_2$ matrix (*classic*), middle: plasmonic $Ag/nTiO_2$ aggregate (*random)* within a $nTiO_2$ or $Zr/nTiO_2$ matrix, and right: plasmonic pure AgNPs as a layer close to the photo anode (coated with a covering *blanket* of TiO_2) on a $nTiO_2$ or $Zr/nTiO_2$ matrix.

In the *random* design, the AgNPs serve both as scattering centers and LSPR field enhancement locations for boosting dye absorption and excitation. Scattering leads to an extension of the interaction length of the incoming light in the photoactive layer, and the amplified evanescent

fields around the AgNPs increase the absorption cross-section effectively. Since the rate of electron excitation in the dye is proportional to the local light intensity,[43] the LSPR field enhancement encourages the creation of more electron-hole pairs, which should lead to a higher photocurrent, and thus increased photovoltaic efficiency.

In the *random* design, the AgNP density in the photoactive material is relatively low, however not homogeneously distributed. Therefore, it is quite possible that some AgNPs are located close to each other within the Ag/nTiO_2 aggregates and create centers of high temperature rise in a matrix with mainly low temperature rise. Mainly small (5°C) to medium (<< 100°C) temperature enhancements are expected. Since the Zr/nTiO_2 is close to the aggregated Ag/nTiO_2 material, the Zr/nTiO_2 is also very close to the outermost AgNPs in the individual aggregates, but further away from the inner AgNPs in the aggregate. Due to the nanoscopic dimensions of the components of the photoactive material components, and the heat conductivity of the nanoscopic materials and the electrolyte, temperature equilibration between Ag/nTiO_2 aggregates and the Zr-doped material should be quickly achieved.

In the *blanket* design, the AgNPs mainly serve as scattering centers to extend the interaction length of the photons to be harvested in the photoactive layer.[44] The LSPR field enhancement is not expected to contribute substantially to the dye absorption in the bulk DSSC as most of the dye molecules are too far away. However, when NPs are positioned at the interface between two dielectrics, light will scatter preferentially into the dielectric with the larger permittivity.[44] The permittivity of TiO_2 ($\varepsilon \sim 100$)[45,46] is higher than that of the polymer (P4VP-10) ($\varepsilon \sim 2.56$)[47] binding the AgNPs to the electrode. Therefore, the incident light is scattered preferentially into the TiO_2 layer. The scattering cross-sections can reach values as high as ten times the geometrical area.[48,49] The AgNP density above the *blanket* (Fig.1) is relatively high and will create locally elevated

temperatures. In the *blanket* design, the Zr/nTiO_2 is relatively far away from the AgNPs and will act on heat mainly due to heat conductivity.

The efficiencies of DSSCs of the three different designs with various AgNP concentrations and Zr concentrations were compared to investigate the influence of the AgNP locations and density, and the effect of Zr-thermo-stabilization.

3 Fabrication of DSSCs

3.1 Materials

The FTO working electrodes, Pt counter-electrodes, polymer gaskets, electrolyte (Iodolyte Z-150), rubber syringes and polymer sealing were all purchased from Solaronix (Aubonne, Switzerland). N719 dye [cis-Bis(isothiocyanato)bis(2,2'-bipyridyl-4,4'-dicarboxylato) ruthenium(II)], terpineol (95 %), titanium(IV) isopropoxide (TIP; 97%), and acetylacetone (acac; > 99%) were purchased from Sigma-Aldrich (Oakville, ON, Canada). Isopropanol (99.5 %), acetonitrile-190 (99.8 %), *N,N*-dimethylformamide (DMF; 99%), and toluene (99.5%) were purchased from Caledon (Georgetown, On, Canada). Anhydrous ethanol was purchased from Commercial Alcohols (Toronto, On, Canada).

Fluorinated tin oxide (FTO) electrodes (thickness, 2.2 mm; sheet resistance, 7 Ω/sq) were purchased from Solaronix (Aubonne, Switzerland). Sulfuric acid (H_2SO_4, 98 %) was purchased from Caledon (Georgetown, On, Canada). Hydrogen peroxide (H_2O_2, 30 wt % in H_2O) and poly(4-vinylpyridine) (P4VP, average MW ~ 60,000 D) were purchased from Sigma-Aldrich (Oakville, ON, Canada). Sparkleen detergent solution was purchased from Fisher Scientific, Ottawa, ON, Canada. Argon was purchased from Praxair, Canada.

Nano-sized $nTiO_2$ (anatase), Zr-doped, nano-sized $Zr/nTiO_2$ (anatase) with 5 and 10 mol % Zr, and $Ag/nTiO_2$, an aggregated, random mixture of AgNPs and $nTiO_2$ (with 2.5 wt.% Ag in the $nTiO_2$ (anatase) and AgNP's Ø < 9 nm) were synthesized via a modified sol-gel route.[32,50-52] In these aggregates, the AgNPs are only partially sealed with TiO_2 thus exhibiting some exposed AgNP surfaces. Pure AgNPs were synthesized according to Evanoff et al.[53]

3.2 Fabrication and assembly of the classic and random design DSSCs

2.5 x 2.5 cm fluorine-doped tin oxide (FTO) glass electrodes (thickness: 2.2 mm; sheet resistance: 7 Ω/sq) were first cleaned in Sparkleen detergent solution to remove residual organic contaminants, followed by deionized water and isopropanol. Between each wash, the electrodes were sonicated for 10 min. The cleaned electrodes were stored in isopropanol and were blown dry using Ar before use. 2 x 2 cm Pt counter-electrodes (thickness: 2 mm) were cleaned in the same manner.

The paste for the photoactive layer was prepared by mixing first powders of $nTiO_2$ (anatase) or $Zr/nTiO_2$ (anatase) with or without an appropriate mass of $Ag/nTiO_2$ (anatase) powder[32,50-52] to obtain 0.3, 0.6, 0.9, 5, 10, 50 and 100 wt.% $Ag/nTiO_2$ containing (Zr-)titania powder. 30 mg of the resulting titania based powder was blended with 0.5 ml of a binder solvent (custom made: 20 % ethyl cellulose in ethanol, terpineol and acetic acid), and the resulting slurry subsequently ground in a mortar with a pestle until a homogeneous gluey consistency was achieved. The photoactive layers were formed by doctor blading a film of paste onto a cleaned FTO glass electrode using a tape template of an area of 0.1257 cm^2, cut with a circular die cutter. The paste was left to dry in

air at room temperature for 30 min, then calcined at 500º C for 1 h. The temperature ramp was set to 15º C/min to avoid surface cracking of the film and to ensure proper adhesion to the FTO glass. After cooling to about 80º C, the photo-electrodes were immersed into a 0.25 mM N719 dye solution containing a 1:1 volume ratio of *tert*-butanol and acetonitrile, and left to immerse for 24h at room temperature. After dyeing, the sensitized photoanodes were washed with anhydrous ethanol to remove any excess of dye molecules to ensure that the porous nTiO_2 film was covered with a monolayer of dye.

After activating the Pt counter-electrodes by heating them on a hotplate at 120º C for a few minutes, the sensitized photo-anodes and the Pt counter-electrodes were assembled in a sandwich-like configuration and sealed with a hot-melt gasket at 120º C. The electrolyte, which contained 150 mM of the iodide/tri-iodide redox couple, was introduced into the cells through a predrilled hole in the counter electrode using a rubber syringe. The Pt electrodes were purchased with one predrilled hole, but a secondary hole was drilled to facilitate air displacement while filling the cell with the electrolyte. Finally, the holes were sealed with a hot-melt polymer and a cover glass (Zeiss, 0.17 mm thickness) to avoid leakage or evaporation of the electrolyte. All fabrication steps were performed under atmospheric conditions. For statistical purposes, 6 cells were fabricated for each sample to ensure reproducibility.

3.3 Preparation of blanket design photo-anodes

In the *blanket* design, pure AgNPs[53] were coated with a thin layer (*blanket*) of TiO_2 by atomic layer deposition (ALD) with a Savannah 100 Cambridge Nanotech (Waltham, Ma, USA) ALD instrument. The TiO_2 *blanket* prevented direct contact between the AgNPs and the electrolyte, avoiding the back reaction of electrons to the redox couple during cell operation. ALD was

implemented here as the method of choice to protect the pure AgNPs with a layer of TiO_2 because it ensures well-defined, conformal growth of TiO_2.

To prepare a *blanket* design electrode, FTO-coated glass electrodes were first cleaned with Piranha solution (3:1 H_2SO_4:H_2O_2) for 30 min at room temperature. This treatment not only removes all organic contaminants from the FTO surface, but also leaves it highly active by introducing hydroxyl groups. Note: This solution reacts violently with most solvents and surfaces, and extreme caution was exercised when carrying out this cleaning step. After the Piranha treatment, the electrodes were thoroughly rinsed with deionized water before being blown dry with Ar gas. The cleaned FTO substrates were functionalized with P4VP by immersing them in an ethanol solution containing 2 wt.% P4VP for 3 h. The electrodes were then rinsed with ethanol to remove any non-adsorbed polymer and heated in an oven for 1 h at 100º C (20º C/min ramp) to relax the monolayer of P4VP, facilitating a homogeneous distribution of the pure AgNPs on the surface. The P4VP-functionalized electrodes were then immersed in the pure AgNP suspension. Having empty d-orbitals characteristic of transition metals, the pure AgNPs in the solution bind strongly to P4VP through the lone pair of electrons on the nitrogen of the pyridine ring. After 12 h of immersion, the AgNP-coated electrodes were rinsed with deionized water and dried with Ar before finally undergoing ALD to create a uniform TiO_2 layer on the AgNPs. To form a pinhole-free (fully protective, fully covering) TiO_2 layer, 300 cycles of TiO_2 precursor were deposited. Alternating 0.1-s pulses of the precursors TIP and H_2O were used to form the TiO_2 layer. A TiO_2 thickness of ~7.7 nm was achieved.[54] The precursors were held in the deposition chamber for 1 s before a 12 s pump. The chamber temperature was set to 200º C, and the N_2 flow rate was 20 sccm. TIP was held at 80º C and all other precursors were used at room temperature.

After the ALD step, the photoactive paste (see sec. *3.2*) was doctor bladed onto the electrode and the DSSC assembled as described above. For statistical purposes, 6 cells of each type were fabricated to ensure reproducibility.

4 Characterization

4.1 General analysis

The photo-anodes of the *blanket* design were characterized with a scanning electron microscope (SEM: LEO-Zeiss 1540 XB, Zeiss, Oberkochen, Germany). A Kratos AXIS Ultra X-ray photoelectron spectrometer (XPS) equipped with a monochromatic Al Kα X-ray source was used to analyze the surface composition of each layer prepared on the photo-anode of the *blanket* design. The LSPR absorption spectra were taken with a Shimadzu UV-3600 UV-Vis-NIR spectrometer. The power conversion efficiency of the cells was measured using the simulated illumination of a Newport Oriel 92250A-1000 (Irvine, Ca, USA) solar simulator and a Keithley 2420 (Cleveland, Oh, USA) digital source meter.

4.2 Characterization of the blanket design DSSC photo-anode

The LSPR peak position (λ_{max}) of the pure AgNPs dispersed in water (refractive index of water: n = 1.33) was at 430 nm. The LSPR peak position in an environment of TiO_2 with a refractive index of at least 2.45 (for anatase)[56-58] is expected to shift considerably towards the red into the visible. The layer system comprising the *blanket* design photo-anode and corresponding SEM images taken throughout the electrode's layer fabrication process are depicted in Fig.2. Fig.2a shows the Piranha treated surface of FTO glass as a polycrystalline, densely agglomerated surface with relatively sharp edged features. The deposition of P4VP smears out the sharp features of the FTO

crystallites (Fig.2b). The deposition of AgNPs and the ALD of TiO_2 leads to indistinguishable SEM images (Fig.2c,d). The AgNPs and the TiO_2 layers are smoothening further the polycrystalline agglomerate structure of the FTO glass electrode and introduce new roundish structures on top of those agglomerates (Ø: 20 - 70 nm), which are interpreted as clustered AgNPs (coated with TiO_2). The density of the AgNPs is very high and comparable to densities of samples investigated by Baffou[24] leading to high expected temperature enhancements in the order of 100°C.

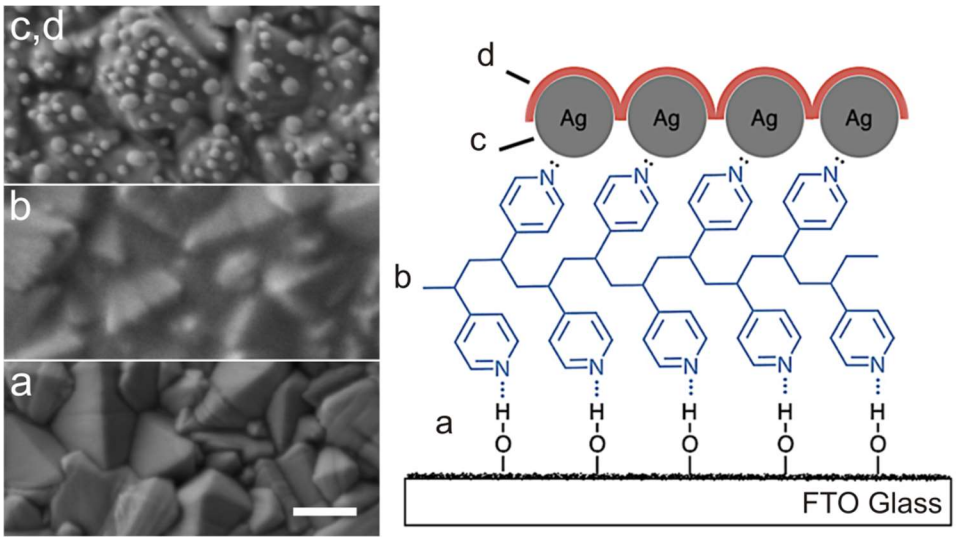

Fig. 2 Scheme of the layer system of the *blanket* design photo-anode and the corresponding SEM images taken throughout the layer-by-layer fabrication process. a) Piranha-treated FTO glass; b) after P4VP-functionalization; c) and d) AgNPs bonded to P4VP and TiO_2 layer deposited via ALD. TiO_2-coated AgNPs are indistinguishable from uncoated AgNPs by SEM. Scale bar in panel 'a' (200 nm) applies to all panels.

XPS was used to confirm the elemental composition of each layer of the electrode, as this technique is well suited to target the top ~10 nm depth of a samples' surface. An XPS survey scan (Fig.3) confirmed the presence of Ag and Ti in the top two layers of the electrode. The spectra of the AgNPs coated surface of the electrode revealed that tin, oxygen, carbon, and small amounts of

nitrogen were present in the sample. The Ag 3d peak appeared after immersing the P4VP-functionalized slides in the AgNP suspensions. The major XPS peaks for the TiO_2-coated surface include Ag 3d, Ti 2p and O 1s. Because 300 cycles of ALD-coated TiO_2 is only ~7.7 nm thick, the spectrometer can still detect the Ag 3d signal, although it was weaker than in the absence of the TiO_2 layer.

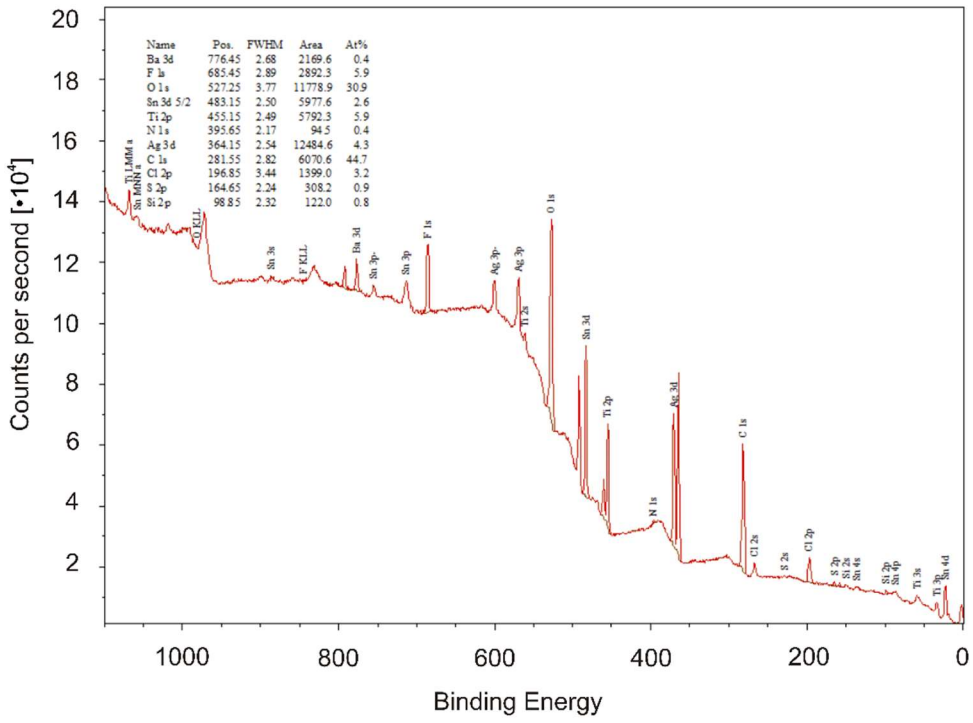

Fig. 3 XPS survey spectrum of sample after ALD (300 cycles TiO_2).

5 Results and Discussion

5.1 Performance of the random design in DSSCs

First, the energy conversion efficiency (η) was studied with respect to the concentration of $Ag/nTiO_2$ present in $Zr/nTiO_2$ photoactive material (10 % Zr) of the DSSCs. The current density-voltage (I-V) curves of the plasmonic *random* design DSSCs with 0.3, 0.6 and 0.9 wt.% of

Ag/nTiO$_2$ concentration are shown in Fig.4. The inset lists the PV characteristics derived from the I-V curves, including the open-circuit voltage (V_{OC}), short-circuit current density (I_{SC}), fill factor (FF) and energy conversion efficiency.[59]

An enhancement of 18 % in energy conversion efficiency (η = 1.24 % → 1.46 %) was found by doubling the Ag/nTiO$_2$ concentration (0.3 wt.% → 0.6 wt.%). Tripling the concentration to 0.9 wt.% resulted in another 9 % increase in efficiency (η = 1.57 %). Even though the AgNPs were partly unprotected, doubling the Ag/nTiO$_2$ concentration increased the photocurrent, a sign of increased carrier extraction. These results imply that the unprotected AgNPs surface in the aggregates was low enough that the benefits from the LSPR outweighed the disadvantage from the exposed AgNP surface acting as recombination sites for electrons.[60,61]

Tripling the Ag/nTiO$_2$ concentration to 0.9 wt.% also showed an improvement in the V_{OC}, but the I_{SC} began to fall. The higher V_{OC} was expected, and reveals that the AgNPs were indeed acting mainly via their LSPR field enhancement as light absorption boosters, generating more efficient electron-hole separation. However, the lack of improvement in the I_{SC} is an indication that the extra charge carriers being created were not extracted efficiently into the external circuit, but rather recombining or quenched, probably at exposed AgNP surfaces.[62] At 0.9 wt.% Ag/nTiO$_2$, the overall unprotected surface area of AgNPs in the photoactive material exceeded a critical value at which undesired electron recombination compensates the advantageous plasmonic assistance.

Further enhancement of the Ag/nTiO$_2$ concentration (I-V data not shown) led to a maximum in η of 1.85 % (at 5 wt.%) but to a substantial drop from η = 1.74 % (at 50 wt.%) to η = 0.69 % (at 100 wt.%). Despite the increasing electron recombination at the unprotected AgNP surfaces, the amount of AgNPs in the photoactive material could be enhanced to 50 wt.% of Ag/nTiO$_2$, translating to a AgNP content of 1.25 wt.% within the photoactive material, a value double as high

as the AgNP content of Qi et al.[21] The main difference of this DSSC system (besides the incomplete shielding of the AgNPs from the electrolyte) to Qi's devices is the presence of Zr in the $nTiO_2$ crystals. The AgNPs are mainly dispersed and should raise the temperature in the photoactive material moderately. However, with increasing AgNP concentration the probability of pairs or larger clusters of AgNPs with small distances, and therefore higher temperature rises, becomes enhanced. The Zr-doping substantially prevented the heat damage, that limited the energy conversion efficiency, at least up to 50 wt.% of $Ag/nTiO_2$.

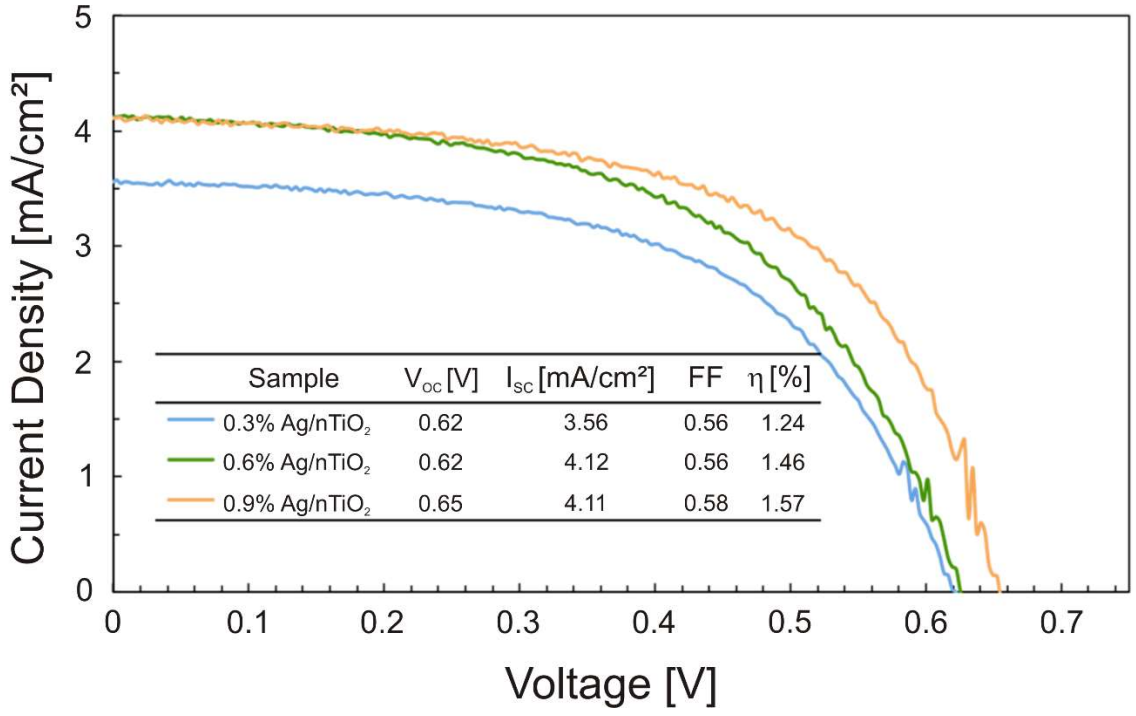

Fig. 4 Current density–voltage curves for DSSCs fabricated with a matrix of 10 mol % $Zr/nTiO_2$ containing various concentrations $Ag/nTiO_2$. The inset shows the DSSC's characteristics calculated from the I-V curves.

In Fig.5 the I-V curve and the PV data for a control sample fabricated with pure $nTiO_2$ as the photoactive material are shown (dotted red line). The efficiency in energy conversion lies here, in the non-plasmonic, non-Zr-doped case, at $\eta = 3.50$ %, which is substantially higher than in the cases using $Ag/nTiO_2$ and $Zr/nTiO_2$ (10% Zr). This is important information. The non-perfect

shielding of the AgNPs from the electrolyte has a destructive impact on η, despite the efficiency stabilization by Zr. It is therefore necessary in the future to take advantage of both the LSPR and the Zr-doping and apply fully protected AgNPs, e.g. as described by Qi et al.[21] in the form of Ag-core/TiO_2 shell NPs.

After determining an "optimum" Ag/nTiO_2 concentration, detailed effects of the Zr-doping, and therefore, the thermal stabilization was tested. Fig.5 relates the efficiency of energy conversion of 4 different DSSCs, the *classic* and the *random* types, fabricated with pure nTiO_2 (control: *classic* design, no plamonics), the Zr/nTiO_2 (5% Zr: *classic* design, no plasmonics,), the Ag/nTiO_2 in nTiO_2 (Ag/nTiO_2: *random* design, plasmonic) as well as the Ag/nTiO_2 in Zr/nTiO_2 (Zr/nTiO_2 + Ag/nTiO_2: *random* design, plasmonic). The Ag/nTiO_2 concentration was kept at 0.6 wt.% (the "optimum") in both DSSC types containing Ag/nTiO_2. The Zr/nTiO_2 contained 5 mol % Zr.[32]

The energy conversion efficiency (Fig.5, inset) systematically increases from the control (η = 3.50 %), to Zr-doping (η = 3.75 %),[32] to applying Ag/nTiO_2 (η = 4.38 %), and finally to η = 6.32 % by applying both Ag/nTiO_2 and Zr/nTiO_2, representing an overall increase of 81% in efficiency from the control. Roughly half of this increase is obtained with the two plasmonic cases, by adding the Zr-doped TiO_2 to Ag/nTiO_2. This significant enlargement of η is reflected by I_{SC} values (Fig.5, inset) which increase parallel to η. An increase in energy conversion efficiency of 7% is found by adding Zr as a thermo-stabilizer to the classic design.[32]

Limiting the AgNP concentration to 0.6 wt.% Ag/nTiO_2 (which translates to 0.015 % Ag in the entire photoactive material) should prevent too many AgNPs in close proximity to each other and, therefore, higher temperature rises. However, the photoactive material is not homogeneous with respect to the AgNP distribution as they are embedded within the aggregates of the Ag/nTiO_2.

Therefore, some AgNPs, which are close to each other, will produce high temperatures. However, these heat contribution is compensated by Zr-doping.

The FF values of the *random* design cells with plasmonics (blue) were lower than those of the AgNP-free cells (red), an outcome which reflects a decreased charge transport within the cell. As mentioned above, energy conversion efficiencies would have been even higher if the AgNPs' surfaces in Ag/nTiO$_2$ would have not been exposed to the electrolyte during cell operation and allowed still for some electron recombination at the "optimum" concentration.

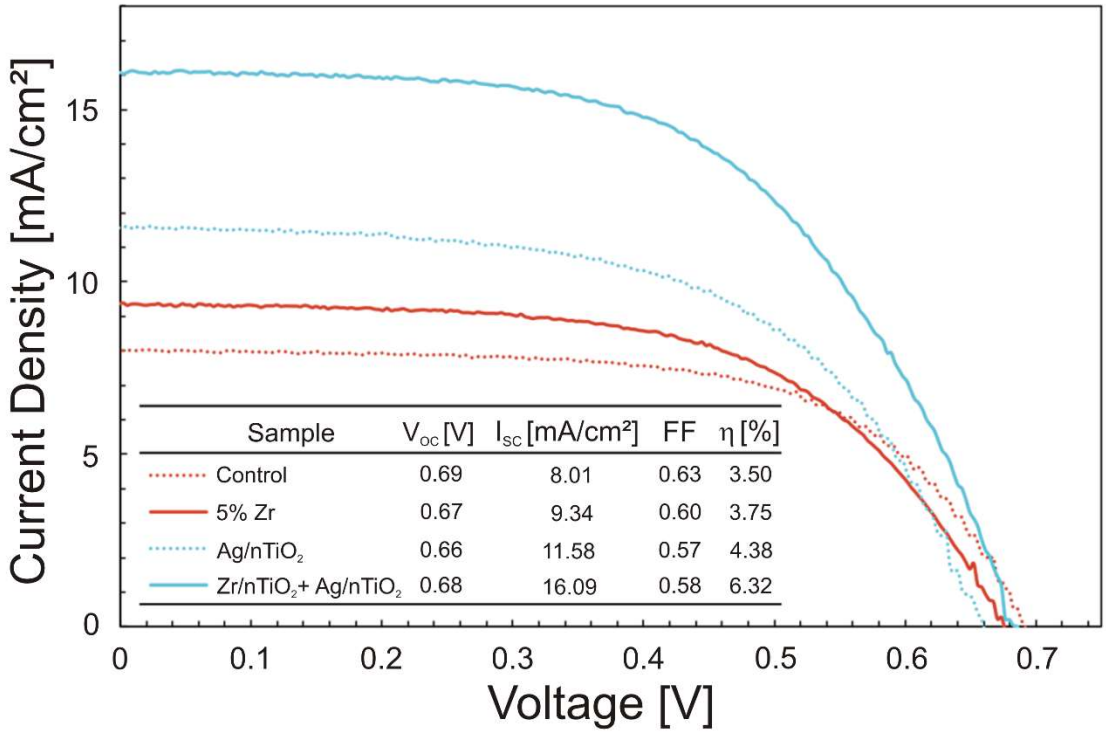

Fig. 5 The effect of Zr/nTiO$_2$ on Ag/nTiO$_2$ containing DSSCs. Measured I-V curves for the *classic* and *random* designed DSSCs in comparison to a control sample (nTiO$_2$). The inset shows the characteristic data calculated from the I-V curves.

5.2 Performance of blanket design in DSSCs

In Fig.6 current-voltage data of *blanket* design DSSCs containing AgNPs are compared to *blanket* design DSSCs without AgNPs. In addition, two non-plasmonic devices, a control and a Zr-containing *classic* DSSC are shown. The figure also stresses the influence on the performance when Zr was incorporated into the photoactive layers of DSSCs provided with a AgNP layer. Note: the Zr-concentration was fixed at 5 mol % Zr in the $nTiO_2$.[32]

First, the data demonstrate that both plasmonic DSSCs (blue) have a higher η than the non-plasmonic devices (red). In addition, and as already discussed for the *random* design DSSCs, doping the non-plasmonic devices with Zr enhanced the efficiency in energy conversion compared to the control.

Moreover, the introduction of the AgNP layer resulted in an η-enhancement of 50 % (η = 3.50 % → 5.25 %), and the addition of $Zr/nTiO_2$ further led to an additional - but very small - increase in η to 5.27 %. The increase due to the pure AgNP layer in DSSCs containing Zr is similar to DSSCs containing no Zr: an enhancement of 40 % was found (from η = 3.75 % → 5.27 %). The overall η-enhancement from a control DSSC to the Zr-containing plasmonic device is 51 %.

The increase in the efficiency of energy conversion is directly correlated to an increase in photocurrent (Fig.6 inset), which corresponds to an enhanced light absorption by the dye. The AgNPs on the photo-anode in the *blanket* design served mainly as a layer of scattering centers to divert the incoming photons and extend the optical path within the cell, thus enhancing the photon interaction and the absorption cross-section within the photoactive cell layer compared to the AgNP-free DSSCs. In short, the dye molecules were reached by photons more often, yet no dyes molecules were located close to the AgNPs in the *blanket* cases. The addition of the $Zr/nTiO_2$, however, did not improve the cell efficiency substantially. The presence of Zr in the photoactive

layer (bulk) had no positive effect on the high heat development expected for the relatively closely-packed AgNPs in the AgNP layer, as the Zr/nTiO_2 material was 'too far away', with the thickness of the ALD TiO_2 layer separating them by at least ~ 7.7 nm. Therefore, thermo-stabilization only occurred efficiently in the non-plasmonic part of the cell.

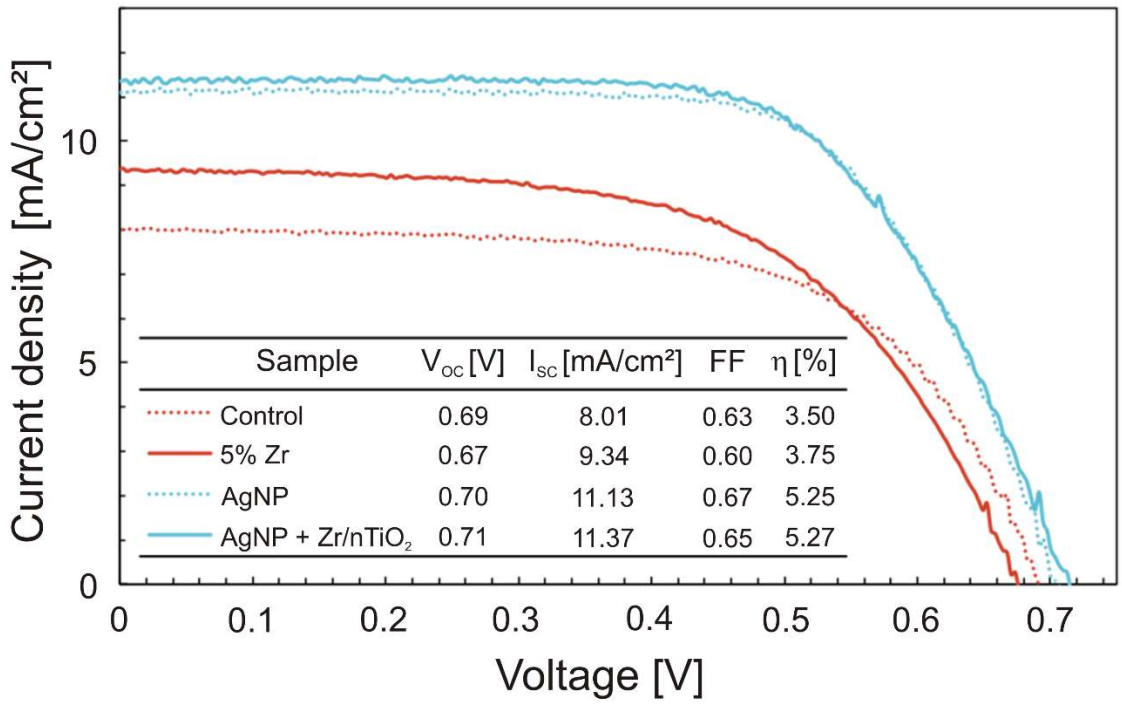

Fig. 6 The effect of Zr and AgNP doping on the I-V curves of the *blanket* design DSSCs in comparison to a control sample of nTiO_2. The inset shows the characteristic data calculated from the I-V curves.

5.3 Comparison between designs

In the following, the performance of the photoactive cell layer designs, *random* and *blanket*, are compared in detail to determine the important performance characteristics and design factors for an optimized cell design when implementing Zr/nTiO_2 as thermo-stabilizers in plamonic DSSCs. First, in contrast to the plasmonic *random* design cells, higher fill factor values were observed in

the *blanket* design cells and in the non-plasmonic cells (Fig.4 and 6, insets). The lower FF values (FF: indicator of electron transport within cells) for cells containing Ag/nTiO_2 is caused by exposed AgNP surfaces, which acted as recombination centers for electrons, preventing them from reaching the exterior circuit. This problem did not appear in the *blanket* design cells. Thus, it is critical to incorporate AgNPs whose surfaces are completely shielded from contact with the electrolyte.

Table 1 provides an overview of all cell designs with respect to Zr and AgNP incorporation.

Table 1. Energy conversion efficiencies with respect to cell design and material application.

Cell Types	**Control**	**Zr/nTiO_2**	**AgNP containing DSSCs**		**AgNP and Zr/nTiO2 containing DSSCs**	
nTiO_2 [mol %]	100	95	100	100	95	95
Zr [*m*ol %.]	-	5	-	-	5	5
Design	*classic*	*classic*	*random*	*blanket*	*random*	*blanket*
η [%]	3.50	3.75	4.38	5.25	6.32	5.27
Δη [%]	0	7	25	50	80	51

In the absence of AgNPs, the incorporation of Zr/nTiO_2 improved the energy conversion efficiency by 7 %. This had been found previously due to stabilization of the anatase crystal structure and an increase in the surface area of the nTiO_2 material.[32] From the two AgNP-containing cell architectures, the *blanket* design achieved the higher efficiency (η = 5.25 %) if Zr/nTiO_2 was absent. However, this does not contribute to better cell design as the AgNP' surfaces in the Ag/nTiO_2 material are partially exposed to electrolyte, and therefore, causes the *random* design to suffer from increased electron recombination. Despite of this shortcoming of the Ag/nTiO_2 material (which can be easily overcome by core-shell AgNPs[21]), the performance of the *random*

design cell surpassed that of the *blanket* design cell when Zr/nTiO_2 was used as the photoactive layer. Energy conversion efficiencies of $\eta = 4.38$ % and $\eta = 6.32$ % were achieved by the *random* design cells and can be improved substantially by a proper AgNP coating strategy.[63] Nonetheless, a clear improvement in efficiency is seen with the inclusion of Zr/nTiO_2, indicating that the addition of Zr helped to provide enhanced thermal stability. The inclusion of Zr in the *blanket* cell design did not increase η considerably (see discussion above).

The ability of Zr/nTiO_2 to thermo-stabilization is only functioning when the AgNPs are dispersed throughout the photoactive Zr/nTiO_2 matrix, as it is given in the *random* design. However, only small to medium concentrations are desired for well functional cells, as the plasmonic thermal behavior creates minor to severe threats with respect to the collapse of the nTiO_2 matrix, which - in turn – reduces the surface area, and consequently the photo-absorption capabilities of the cell.

Zr exhibited thermo-stabilization in both AgNP-containing cell designs, but was more effective in the *random* design. The drawback of the *blanket* design is that the enhanced local field from the LSPR only enhanced charge separation for a very limited number of dye molecules located very close to the AgNPs below the 'blanket', finally leading to only a limited photocurrent enhancement. The enhanced photocurrent observed in the *blanket* design cells can thus, in contrast to the control, be mainly attributed to plasmonic scattering (where AgNPs acted as scattering centers), enhancing the interaction of the incoming light with the photoactive layer and the dye molecules. Therefore, the *random* design is the superior cell design for incorporating AgNPs in combination with Zr/nTiO_2 photoactive material in DSSCs.

6 Conclusions

The use of Zr/nTiO_2 as a thermo-stabilizing material in the photoactive layer of DSSCs was investigated for stabilizing nTiO_2 when jeopardized by the plasmonic heat generation created from the presence of AgNPs, whose purpose served to enhance the energy conversion efficiency of the cells. In both cell architectures, the AgNPs were used as field enhancers and scattering centers to more efficiently excite the dye molecules.

The results showed that Zr exhibited thermo-stabilizing properties in both plasmonic cell architectures. The *random* design, consisting of AgNPs dispersed throughout the photoactive layer, demonstrated superior performance over the *blanket* design in the presence of Zr/nTiO_2. Both the photocurrent and fill factor were significantly enhanced, and an energy conversion efficiency increase of 44 % was observed in the *random* design when incorporating Zr into the nTiO_2 photoactive matrix. The DSSC's performance can be additionally enhanced via an appropriate coating to avoid electron recombination. This should also lead to individual AgNPs, which can be easier and more evenly dispersed throughout the photoactive layer than the aggregated Ag/nTiO_2 material. Zr did not play a significant role in improving the energy conversion efficiency of *blanket* design DSSCs, as its thermo-stabilizing benefits was limited in this architecture.

It can therefore be concluded that the *random* design is the better cell design for a combined incorporation of AgNPs and Zr/nTiO_2 in DSSCs. It also can be concluded that the *random* design is the overall best alternative for LSPR-enhanced DSSCs. This design allows both plasmonic features, the scattering and the field enhancement, can both contribute most optimally to the energy conversion efficiency. Therefore, it is important to investigate the threshold concentration of

AgNPs in a Zr-doped TiO_2 matrix at which the enhancing plasmonic features are overtaken by disadvantages from too many AgNPs.

Zr's thermo-stabilizing effect in plasmon-enhanced DSSCs can lead to new solar cell designs with smaller semiconductor thicknesses, and thus lower material costs and quicker investment amortization.

7 Acknowledgement

The authors would like to thank NSERC Strategic and Discovery programs for financial aid, and the Western Nanofabrication Facility and Surface Science Western for electron microscopy and XPS analysis. Jian Liu in Andy Sun's lab at Western is thanked for atomic layer deposition and William Xu for UV-Vis spectra.

References

(1) J. Wu, . Lan, J. Lin, M. Huang, Y. Huang, L. Fan and G. Lou, "Electrolytes in dye-sensitized solar cells," *Chem. Rev.* **115**(5)*,* 2136–2173 (2015).

(2) A. Fakharuddin, R. Jose, T.M. Brown, F. Fabregat-Santiago and J.A. Bisquert, "Perspective on the production of dye-sensitized solar modules,". *Energy Environ. Sci.* **7,** 3952–3981 (2014**).**

(3) A. Kojima, K. Teshima, Y. Shirai and T. Miyasaka, "Organometal halide perovskites as visible-light sensitizers for photovoltaic cells," *J. Am. Chem. Soc.* **131**(17)*,* 6050–6051 (2009).

(4) J.-H. Im, C.-R. Lee, J.-W. Lee, S.-W. Park and N.-G. Park, "6.5% Efficient perovskite quantum-dot-sensitized solar cell," *Nanoscale***, 3**, 4088-4093 (2011).

(5) H. Hu, J. Shen, X. Cao, H. Wang, H. Lv, Y. Zhang, W. Zhu, J. Zhao and C. Cui, "Photo-assisted deposition of Ag nanoparticles on branched TiO_2 nanorod arrays for dye-sensitized solar cells with enhanced efficiency," *Journal of Alloys and Compounds* **694***,* 653-661 (2017).

(6) M.J. Yun, S.I. Cha, S.H. Seo and D.Y. Lee, "Highly flexible dye-sensitized solar cells produced by sewing textile electrodes on cloth," *Sci. Rep.* **4***,* 5322 (2014).

(7) W.-Q. Wu, Y.-F. Xu, H.-S. Rao, , C.-Y. Su and D.-B. Kuang, "A tri-layered photoanode of TiO_2 nanoparticles on 1D-3D nanostructured TiO_2 - Grown flexible Ti substrate for high-efficiency (9.1%) dye-sensitized solar cells with unprecedentedly high photocurrent density," *J. Phys. Chem. C*, **118**(30), 16426-16432 (2014)..

(8) L. Ming, H. Yang, W. Zhang, X. Zeng, D. Xiong, Z. Xu, H. Wang, W. Chen, X. Xu, M. Wang, J. Duan, Y.-B. Cheng, J. Zhang, Q. Bao, Z. Wei, S. Yang, "Selective laser sintering of TiO_2 nanoparticle film on plastic conductive substrate for highly efficient flexible dye-sensitized solar cell application," *J. Mater. Chem. A* **2**(13), 4566-4573 (2014).

(9) Yamaguchi, T.; Tobe, N.; Matsumoto, D.; Nagai, T.; Arakawa, H. Highly efficient plastic-substrate dye-sensitized solar cells with validated conversion efficiency of 7.6%," *Sol. Energy Mater. Sol. Cells* **94**(5), 812–816 (2010).

(10) M. Eslamian, "Spray-on thin film PV solar cells: Advances, potentials and challenges," *Coatings* **4**(1), 60–84 (2014).

(11) A. Hagfeldt, G. Boschloo, L. Sun, L. Kloo and H. Pettersson, "Dye-sensitized solar cells," *Chem. Rev.* **110**(11)*,* 6595–663 (2010).

(12) H. A. Atwater and A. Polman, "Plasmonics for improved photovoltaic devices," *Nat. Mater.*, **9***,* 205–213 (2010).

(13) C. Chen, M. Wang, J.-Y. Li, N. Pootrakulchote, L. Alibabaei, , C.-H. Ngoc-Le, J.-D. Decoppet, J.-H. Tsai, C. Grätzel, C.-G. Wu,. S.M. Zakeeruddin, M. Grätzel, "Highly efficient light-harvesting ruthenium sensitizer for fhin-film dye-sensitized solar cells," *ACS Nano*, **3**(10)*,* 3103–3109 (2009).

(14) P. Mandal and S. Sharma, "Progress in plasmonic solar cell efficiency improvement: A status review," *Renewable and Sustainable Energy Reviews* **65***,* 537-552 (2016).

(15) T. Jensen, L. Kelly, A. Lazarides and G.C. Schatz, "Electrodynamics of noble metal nanoparticles and nanoparticle clusters," *Journal of Cluster Science,* **10**(2) 295–317 (1999).

(16) S.K. Cushing and N.Wu, "Plasmon-enhanced solar energy harvesting," *Electrochem. Soc. Interface* **2***,* 63–67 (2013).

(17) S. Linic, P. Christopher and D.B. Ingram, "Plasmonic-metal nanostructures for efficient conversion of solar to chemical energy," *Nat. Mater.*, **10***,* 911–921 (2011).

(18) Q. Xu, F. Liu, W. Meng and Y. Huang, "Plasmonic core-shell metal-organic nanoparticles enhanced dye-sensitized solar cells," *Optics Express*, **20**(S6)*,* 898–907 (2012).

(19) Q. Xu, F. Liu, Y. Liu, F. Cui, X. Feng, W. Zhang and Y. Hunag, "Broadband light absorption enhancement in dye-sensitized solar cells with Au-Ag alloy popcorn nanoparticles," *Sci. Rep.*, **3***,* 2112-1-7 (2013).

(20) X. Dang, J. Qi, M.T. Klug, P.-Y. Chen, D.S. Yun, N.X. Fang, P.T. Hammond and A.M. Belcher, "Tunable localized surface plasmon-enabled broadband light-harvesting enhancement for high-efficiency panchromatic dye-sensitized solar cells," *Nano Lett.*, **13**(2)*,* 637–42 (2013).

(21) J. Qi, X. Dang, P.T. Hammond and A.M. Belcher, "Highly efficient plasmon-enhanced dye-sensitized solar cells through metal@oxide core-shell nanostructure," *ACS Nano* **5**(9), 7108–7116 (2011).

(22) L.A. Austin, M.A. Mackey, E.C. Dreaden and M.A. El-Sayed, "The optical, photothermal, and facile surface chemical properties of gold and silver nanoparticles in biodiagnostics, therapy, and drug delivery," *Archives of Toxicology* **88**(7), 1391-1417 (2014).

(23) G. Baffou and R. Quidant, "Thermo-plasmonics: using metallic nanostructures as nano-sources of heat," *Laser Photonics Rev*. **7**(2), 171–187 (2013).

(24) G. Baffou, P. Bon, J. Savatier, J. Polleux, M. Zhu, M. Merlin, H. Rigneault and S. Monneret, "Thermal imaging of nanostructures by quantitative optical phase analysis," *ACS Nano* **6**(3), 2452–2458 (2012).

(25) I.N. Obotowo, I.B. Obot and U.J. Ekpe, "Organic sensitizers for dye-sensitized solar cell (DSSC): Properties from computation, progress and future perspectives," *Journal of Molecular Structure* **1122,** 80-87 (2016).

(26) K. Hara, and N. Koumura, "Organic dyes for efficient and stable dye-sensitized solar cells," *Material Matters,* **4**(4), 92-98 (2009).

(27) Y. Qin and Q. Peng, "Ruthenium sensitizers and their applications in dye-sensitized solar cells," *International Journal of Photoenergy* **2012**, 291579-1-21 (2012).

(28) O. Kohle, M. Grätzel, A.F. Meyer and T.B. Meyer, "The photovoltaic stability of bis(isothiocyanato)ruthenium(II)-bis-2,2_-bipyridine-4,4_- dicarboxylic acid and related sensitizers," *Advanced Materials*. **9**(11), 904–906 (1997).

(29) S. Hassing, K.D. Jernshøj, P. T. Nguyen and T. Lund, "Investigation of the Stability of the Ruthenium-based dye (N719) utilizing the polarization properties of dispersive Raman modes and/or of the fluorescent emission," *J. Phys. Chem. C*, **117**(45), 23500−23506 (2013).

(30) S. Sarker, H.W. Seo and D.M. Kim, "Electrochemical impedance spectroscopy of dye-sensitized solar cells with thermally degraded N719 loaded TiO_2," *Chemical Physics Letters* **585**, 193–197 (2013).

(31) A.P. Bell, J.A. Fairfield, E.K. McCarthy, S. Mills, J.J. Boland, G. Baffou and D. McCloskey, "Quantitative study of the photothermal properties of metallic nnowire networks," *ACS Nano* **9**(5), 5551–5558 (2015).

(32) A. Pasche, B. Grohe, S. Mittler and P.A. Charpentier, "Zr-doped TiO_2 nanoparticles synthesized via a sol-gel route and their application in dye-sensitized solar cells for thermo-stabilization, Materials Research Express (2017) https://doi.org/10.1088/2053-1591/aa742d.

(33) M. Dürr, S. Rosselli, A. Yasuda and G. Nelles, "Band-gap engineering of metal oxides for dye-sensitized solar cells," *J. Phys.Chem. B* **110**(43)**,** 21899–21902 (2006).

(34) A. Kitiyanan, S. Sakulkhaemaruethai, Y. Suzuki and S.Yoshikawa, "Structural and photovoltaic properties of binary TiO_2-ZrO_2 oxides system prepared by sol-gel method," *Compos. Sci. Technol.*, **66***,* 1259–1265 (2006).

(35) M.D. Hernández-Alonso, I. Tejedor-Tejedor,J.M. Coronado, J. Soria and M.A. Anderson, "Sol-gel preparation of TiO_2-ZrO_2 thin films supported on glass rings: influence of phase composition on photocatalytic activity," *Thin Solid Films* **502**(1-2), 125–131 (2006).

(36) D.J. Reidy, J.D. Holmes and M.A. Morris, "Preparation of a highly thermally stable titania anatase phase by addition of mixed zirconia and silica dopants," *Ceram. Int.* **32***,* 235–239 (2006).

(37) R.A. Lucky and P.A. Charpentier, "A one-step pproach to the synthesis of ZrO_2-modified TiO_2 nanotubes in supercritical carbon dioxide," *Adv. Mater.* **20**(9)*,* 1755–1759 (2008).

(38) R.A. Lucky, Y. Medina-Gonzalez and P.A. Charpentier, "Zr doping on one-dimensional titania nanomaterials synthesized in supercritical carbon dioxide," *Langmuir* **26**(24)*,* 19014–19021 (2010).

(39) B. Paci, A. Generosi, V.R. Albertini, G.D. Spyropoulos, E. Stratakis and E. Kymakis, "Enhancement of photo/thermal stability of organic bulk heterojunction photovoltaic devices via gold nanoparticles doping of the active layer," *Nanoscale* **4***,* 7452-7459 (2012).

(40) S. Link and M.A. El-Sayed, "Size and temperature dependence of the plasmon absorption of colloidal gold nanoparticles," *J. Phys. Chem. B* **103**(21), 4212-4217 (1999).

(41) Z. Miao, L. Xu, H. Song, H. Zhao and L.Chou, "One-pot synthesis of ordered mesoporous irconium oxophosphate with high thermostability and acidic properties," *Catal. Sci. Technol.* **3***,* 1942-1954 (2013).

(42) F. Namavar, G. Wang, C.L. Cheung, R.F. Sabirianov and X.C. Zeng, "Thermal stability of nanostructurally stabilized irconium oxide," *Nanotechnology*, **18***,* 415702-1-6 (2007).

(43) M.K. Kumar, S. Krishnamoorthy, L.K. Tan, S.Y. Chiam, S. Tripathy and H. Gao, "Field effects in plasmonic photocatalyst by precise SiO_2 thickness control using atomic layer deposition," *ACS Catal.*, **1**(4)*,* 300–308 (2011).

(44) J. Mertz, "Radiative absorption, fluorescence, and scattering of a classical dipole near a lossless interface: a unified description," *J. Opt. Soc. Am. B* **17**(11)*,* 1906-1913 (2000).

(45) S. Marinel, D.H. Choi, R. Heuguet, D. Agrawal and M. Lanagan, "Broadband dielectric characterization of TiO_2 ceramics sintered through microwave and conventional processes," *Ceram. Int.*, **39***,* 299–306 (2013).

(46) Z. Ahmad, "Polymeric dielectric materials," Chap. 1 in *Engineering, Electrical and Electronic Engineering, Dielectric Media*, M.A. Silaghi, Ed., InTech, (2012), DOI:10.5772/50638

(47) S. Scheinert, G. Paasch, I. Hörselmann and A. Herasimovich, "Low-cost submicrometer organic field-effect transsistors," Chap.6 in *Advances in Polymer Sciences, Organic Electronics,* **223,** T. Grasser, G. Meller, L. Li, Eds., pp. 155-188, Springer: Berlin, Heidelberg, Germany, (2010).

(48) K.R. Catchpole and A. Polman, "Design principles for particle plasmon enhanced solar cells," *Appl. Phys. Lett.* **93**(19), 191113-1-3 (2008).

(49) C.F. Bohren and D.R. Huffman, *Absorption and scattering of light by small particles,* Wiley, New York, USA (1983).

(50) Anastasia Pasche, Doping plasmon-enhanced TiO_2 with zirconia to improve solar energy harvesting in dye-sensitized solar cells, Master Thesis, The University of Western Ontario, Canada (2015).

(51) Y. Chen, S. Zhou, G. Gu and L. Wu, "Microstructure and properties of polyester-based polyurethane/titania hybrid films prepared by sol–gel process," *Polymer* **47**(5), 1640–48 (2006).

(52) R. Sui and P.A. Charpentier, "Synthesis of metal oxide nanostructures by direct sol-gel chemistry in supercritical fluids," *Chem. Rev.* **112**(6)**,** 3057–82 (2012).

(53) D.D. Evanoff and G. Chumanov, "Size-controlled synthesis of nanoparticles. 1. 'Silver Only' aqueous suspension via hydrogen reduction," *J. Phys. Chem. B*, **108**(37), 13948-13956 (2004).

(54) S.D. Standridge, G.C. Schatz and J.T. Hupp, "Toward plasmonic solar cells: Protection of silver nanoparticles via atomic layer deposition of TiO_2," *Langmuir*, **25**(5), 2596–2600 (2009).

(56) J.G. Liu, Y. Nakamura, T. Ogura, Y. Shibasaki, S. Ando and M. Ueda, "Optically transparent sulfur-containing polyimide-TiO_2 nanocomposite films with high refractive index and negative pattern formation from poly(amic acid) -TiO_2 nanocomposite film," *Chem. Mater.*, **20**(1)*,* 273–281 (2008).

(57) A. Herman, Y.B. Liu, J.X. Xue, J. Wang, H.I. Elim, W. Ji, Y. Lic and T.J. White, "Controlling the crystallinity and nonlinear optical properties of transparent TiO_2–PMMA nanohybrids," *J. Mater. Chem.* **14**, 2978-2987 (2004).

(58) H. Tang, H. Berger, P.E. Schmid and F. Levy, "Optical properties of anatase (TiO_2)," *Solid State Communication* **92**(3), 267-271 (1994).

(59) J.A. Mazer, *Solar cells: an introduction to crystalline photovoltaic technology*, Kluwer Academic Publishers: Boston , USA (1997).

(60) L.M. Santos, W.A. Machado, M.D. França, K.A. Borges, R,M. Paniago, A.O.T. Patrocinio, A.E.H. Machado, "Structural characterization of Ag-doped TiO_2 with enhanced photocatalytic activity," *RSC Adv*. **5**(125), 103752–103759 (2015).

(61) Y. Huang, Z. Xuxu, Y. Zhongyi, T. Feng, F. Beibei and H. Keshan, „Preparation of nitrogen-doped TiO_2 nanoparticle catalyst and its catalytic activity under visible light," *Chin. J. Chem. Eng***. 15**(6), 802–807 (2007).

(62) C.T. Yip, X. Liu, Y. Hou, W. Xie, J. He, S. Schlücker, D.Y. Lei and H. Huang, "Strong competition between electromagnetic enhancement and surface-energy-transfer induced

quenching in plasmonic dye-sensitized solar cells: A generic yet controllable effect,". *Nano Energy*, **26**, 297-304 (2016).

(63) R.T. Tom, A.S. Nair, N. Singh, M. Aslam, C.L. Nagendra, R. Philip, K. Vijayamohanan and T. Pradeep, "Freely dispersible Au@TiO_2, Au@ZrO_2, Ag@TiO_2, and Ag@ZrO_2 core−shell nanoparticles: One-step synthesis, characterization, spectroscopy, and optical limiting properties," *Langmuir* **19**(8), 3439 – 3445 (2003).

FIGURE CAPTIONS

Fig. Schemes of the three DSSC designs. Left: non-plasmonic AgNP-free $nTiO_2$ or $Zr/nTiO_2$ matrix (*classic*), middle: plasmonic $Ag/nTiO_2$ aggregate (*random)* within a $nTiO_2$ or $Zr/nTiO_2$ matrix, and right: plasmonic pure AgNPs as a layer close to the photo anode (coated with a covering *blanket* of TiO_2) on a $nTiO_2$ or $Zr/nTiO_2$ matrix.

Fig.2 Scheme of the layer system of the *blanket* design photo-anode and the corresponding SEM images taken throughout the layer-by-layer fabrication process. a) Piranha-treated FTO glass; b) after P4VP-functionalization; c) and d) AgNPs bonded to P4VP and TiO_2 layer deposited via ALD. TiO_2-coated AgNPs are indistinguishable from uncoated AgNPs by SEM. Scale bar in panel 'a' (200 nm) applies to all panels.

Fig.3 XPS survey spectrum of sample after ALD (300 cycles TiO_2).

Fig.4 Current density–voltage curves for DSSCs fabricated with a matrix of 10 mol % $Zr/nTiO_2$ containing various concentrations $Ag/nTiO_2$. The inset shows the DSSC's characteristics calculated from the I-V curves.

Fig.5 The effect of $Zr/nTiO_2$ on $Ag/nTiO_2$ containing DSSCs. Measured I-V curves for the *classic* and *random* designed DSSCs in comparison to a control sample ($nTiO_2$). The inset shows the characteristic data calculated from the I-V curves.

Fig.6 The effect of Zr and AgNP doping on the I-V curves of the *blanket* design DSSCs in comparison to a control sample of $nTiO_2$. The inset shows the characteristic data calculated from the I-V curves.